A comparative study of the effects of CuO, NiO, ZrO₂ and CeO₂ coupling on the photocatalytic activity and characteristics of ZnO

Eluvathingal Devassy Sherly*, John Judith Vijaya*,†, Lourdusamy John Kennedy,
Arunachalam Meenakshisundaram***, and Melcureraj Lavanya*****

*Catalysis and Nanomaterials Research Laboratory, Department of Chemistry, Loyola College, Chennai 600 034, India
**Materials Division, School of Advanced Sciences, Vellore Institute of Technology (VIT) University,
Chennai Campus, Chennai 600 127, India
***R&D Division, Chennai Petroleum Corporation Limited, Manali, Chennai 600 068, India

Abstract−ZnO nanoparticles were coupled with CuO, NiO, ZrO₂ and CeO₂ in 2 : 1 molar ratio by a microwave assisted one pot solution combustion synthesis. Structural, morphological and optical properties of ZnO and coupled oxides were investigated by X-ray diffraction (XRD), field emission scanning electron microscopy (FESEM), transmission electron microscopy (TEM), energy dispersive X-ray spectroscopy (EDX), UV-Vis diffuse reflectance spectroscopy (DRS), photoluminescence spectroscopy (PL), Fourier transform infrared (FTIR) spectroscopy and Brunauer-Emmett-Teller (BET) surface area analysis. XRD data revealed the presence of two phases in the coupled oxides. Photocatalytic activity of pure ZnO and ZnO coupled oxides was compared for the degradation of 2,4-dichlorophenol (2,4-DCP) under near UV light (365 nm) irradiation and the rate constant (k) values were calculated from the kinetic studies. The coupled oxide, Zn₂Ce with ZnO and CeO₂ in 2 : 1 molar ratio showed maximum degradation efficiency due to the efficient interparticle electron transfer between ZnO and CeO₂.

Keywords: Combustion Synthesis, Coupled Metal Oxides, Semiconductor, Photocatalytic Degradation, Interparticle Electron Transfer

INTRODUCTION

ZnO is a good semiconducting material for photocatalytic applications, due to its unique chemical and physical properties, environmental stability and low cost, as compared to other nanosized metal oxides. But ZnO can only operate under UV light irradiation because of its wide band gap (3.2 eV). Moreover, the recombination of the photogenerated electron-hole pairs (e⁻/h⁺) occurs quickly on a time scale of 10^{-9} to 10^{-12} s [1-3]. Number of approaches have been tried to improve the photocatalytic activity of ZnO for the degradation of organic compounds in water and air like doping with metals and nonmetals [4,5], dye sensitizing [6,7] and coupling with other metal oxides [8-10]. Generation of surface defects and graphene and g-C₃N₄ hybridization are yet other ways of improving the photocatalytic efficiency of ZnO [11-17].

Surface defects, such as, oxygen vacancies and interstitial oxygen atoms, play an important role in improving the photocatalytic performance of ZnO. ZnO with high levels of surface defects showed improved photocatalytic performance as the photogenerated charge carriers can be trapped by the surface defects, thus facilitating the separation of photogenerated e⁻/h⁺ pairs. The defects can also narrow ZnO band gap and enhance the visible light photocatalytic activity [11,12]. Graphene-semiconductor composites have attracted

much attention for photocatalysis, as coupling of semiconductors, such as, ZnO with graphene and graphitic carbon nitride (g-C₃N₄) can reduce the semiconductor band gap and shift the absorption edge to visible and near-IR regions. The high charge carrier mobility and high specific surface area that graphene possesses can significantly improve the separation efficiency of the photogenerated e⁻/h⁺ pairs and increase the number of reactive sites during the photocatalytic process [13-17].

Coupling of two or more metal oxides with suitable valence and conduction band edges can facilitate the interparticle e⁻/h⁺ transfer and thus reduce e⁻/h⁺ recombination and increase photocatalytic efficiency. Coupling between two semiconductors with appropriate band positions can also extend the photo-response range to visible light and shift the photocatalytic process to ordinary solar light as major portion of solar light is composed of visible light [18-20].

In the present study, we prepared ZnO and MO coupled ZnO (MO=CuO, NiO, ZrO₂ and CeO₂), by a microwave assisted solution combustion synthesis (SCS). SCS is an effective, low-cost method for the production of various industrially important nanomaterials. This process involves a self-sustained reaction in homogeneous solution of different oxidizers (e.g., metal nitrates) and fuels (e.g., urea, glycine, hydrazides) [21,22]. Many types of combustion synthesis exist which differ mainly in the physical state of the reactants or in the combustion modality [23]. We have adapted the urea-nitrate combustion synthesis, in which the fuel is urea and metal nitrates are oxidant, and the reaction is carried out in a microwave oven. Microwave heating has been developed into an

efficient method for the fabrication of nanomaterials. Microwave irradiation is electromagnetic radiation in the frequency range 0.3 to 300 GHz which corresponds to wavelengths of 1 mm to 1 m. Microwave irradiation induces interaction of the dipole moment of polar molecules with alternating electronic and magnetic fields, causing molecular-level heating which leads to homogeneous and quick thermal reactions with low thermal gradients. The reaction can be performed in a domestic microwave oven (of 2.45 GHz, corresponding to a wavelength of 12.24 cm) and the operation is clean, fast, less energy consuming, without the use of any harmful organic solvents.

As-prepared ZnO and the coupled oxides - Zn_2Cu, Zn_2Ni, Zn_2Zr and Zn_2Ce with ZnO and MO (MO=CuO, NiO, ZrO_2 and CeO_2) in 2 : 1 molar ratio were used for the photocatalytic degradation of 2,4-dichlorophenol (2,4-DCP) under near UV light (365 nm) irradiation. 2,4-DCP is a precursor in the manufacture of the widely used herbicide, 2,4-dichlorophenoxy acetic acid (2,4-D) and is also the major transformation product of 2,4-D. It is one of the 129 priority pollutants listed by the United States EPA, because of its carcinogenicity, toxicity and persistence [24-26]. The relationship between the photocatalytic activity and the structural features of the prepared catalysts was investigated and the coupled metal oxide, Zn_2Ce showed maximum efficiency in the degradation of 2,4-DCP on irradiation with near UV light (365 nm) compared to ZnO and other coupled oxides.

EXPERIMENTAL

1. Synthesis of Nano ZnO, and Coupled ZnO (Zn_2Cu, Zn_2Ni, Zn_2Zr and Zn_2Ce)

All the reagents used were of analytical grade obtained from Merck, India and were used as received without further purification. The stoichiometric compositions of the solution components (fuels and oxidizer) were calculated according to the principle of propellant chemistry, keeping the oxidizer (metal nitrate) to fuel (urea) ratio as unity. For the preparation of ZnO nanoparticles, Zinc nitrate and urea in stoichiometric ratio were dissolved separately in deionized water, mixed and stirred for one hour to obtain a clear solution. This was transferred to a silica crucible and heated in a domestic microwave-oven (2.45 GHz and 850 W) for 7 minutes. Initially, the solution boiled and underwent dehydration followed by decomposition with the evolution of gases. When the solution reached the point of spontaneous combustion, it vaporized and instantly became a solid. The obtained solid was washed well with distilled water and ethanol and dried in a hot air oven at 80 °C for 2 h. Other individual metal oxides, CuO, NiO, ZrO_2 and CeO_2 were prepared by the same method using the respective metal nitrates. For the synthesis of coupled oxides, ZnO-MO (where MO=CuO, NiO, ZrO_2 and CeO_2), zinc nitrate and the other respective metal nitrate ($Cu(NO_3)_2$, $Ni(NO_3)_2$, $ZrO(NO_3)_2$ and $Ce(NO_3)_3$) in 2 : 1 molar ratios were dissolved in deionized water and mixed with required amount of urea and treated in a microwave oven for 7 minutes. The prepared coupled metal oxides were labeled as Zn_2Cu, Zn_2Ni, Zn_2Zr and Zn_2Ce.

2. Characterization of ZnO and ZnO-MO$_x$

The crystallinity of pure ZnO and ZnO-MO was determined by using a Philips X'pert X-ray diffractometer with Cu Kα radiation at λ=1.540 Å. Morphological studies and energy dispersive X-ray analysis were done with a Hitachi S-4800 field emission scanning electron microscope. TEM images were captured with TECNAI FE12 TEM instrument operating at 120 kV. The FT IR spectra were recorded on Bruker Tensor 27 FTIR spectrophotometer at scanning range from 400 to 4,000 cm^{-1}. The diffuse reflectance UV-Visible spectra of the samples were recorded by a Cary 100 UV-Visible spectrophotometer to estimate their optical band gap. The room temperature photoluminescence (PL) studies were done using the Varian Cary Eclipse fluorescence spectrophotometer. BET surface areas of the photocatalysts were measured using an automatic adsorption instrument (Quantachrome Corp. Nova-1000 gas sorption analyzer).

3. Photocatalytic Reactor Setup and Degradation Procedure

Photocatalytic degradation (PCD) experiments were carried out in a multilamp photocatalytic reactor (Heber Scientific), as shown in Fig. 1. The lamp housing consisted of medium-pressure mercury lamps (8×8 W) emitting 365 nm light of intensity 2,650 μW/cm^2 with polished anodized aluminium reflectors and black cover to prevent UV leakage. The top portion of the reactor has ports for sampling, gas-purging, and gas outlet. A fixed amount (50 mg) of pure ZnO or coupled metal oxide was added to 100 mL of 2,4-DCP aqueous solution (50 mgL^{-1}). The above slurry was stirred for 30 min in the dark to reach the adsorption/desorption equilibrium followed by near UV light irradiation in the photocatalytic reactor. Aliquots (3 mL) were withdrawn from the suspension at specific time intervals and centrifuged immediately at 1,500 rpm. The extent of 2,4-DCP degradation was monitored by using a UV-Visible spectrophotometer (Perkin-Elmer, Lambda 25). The PCD efficiency (η) was calculated from the following expression: $\eta=((C_0-C_t)/C_0)\times100$ where, C_0 is the initial concentration of 2,4-DCP, and C_t, the concentration of 2,4-DCP after time 't'. To check the stability and reusability of the catalyst, the resulting suspen-
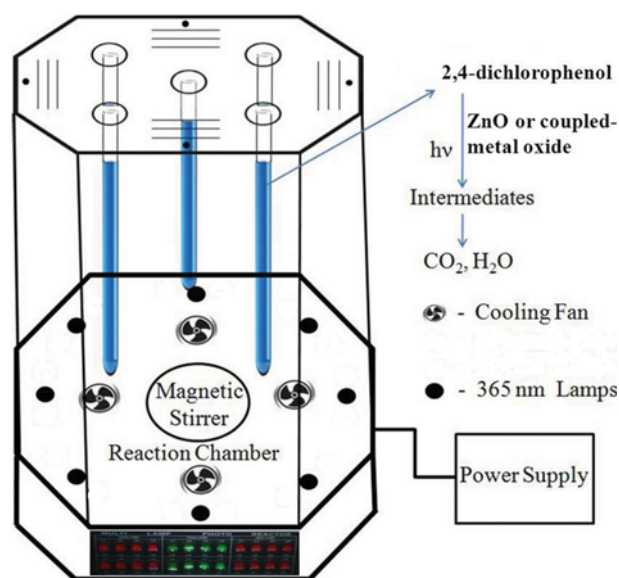

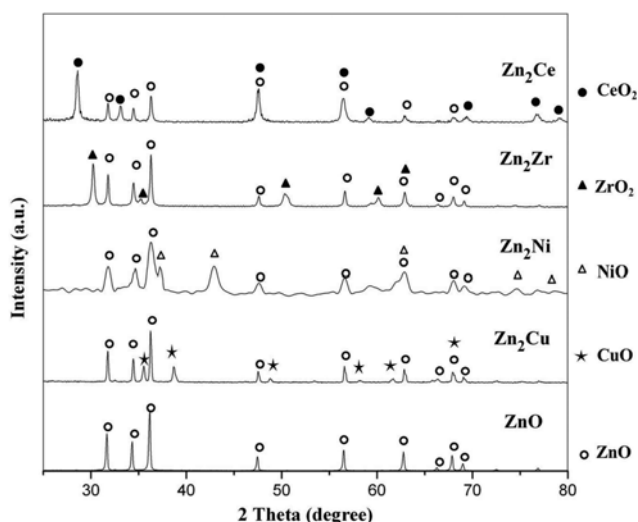**Fig. 1. Schematic diagram of the photocatalytic reactor used in the present study.**

Fig. 2. XRD pattern of ZnO and the coupled oxides Zn₂Cu, Zn₂Ni, Zn₂Zr , Zn₂Ce samples.

sion was centrifuged at the end of the experiment. The separated catalyst was reused for repeated tests. All measurements were repeated twice and the results were reproducible within the experimental errors (±3%).

RESULTS AND DISCUSSION

1. Catalyst Characterization

1-1. XRD Analysis

The crystal structure of pure ZnO and coupled ZnO nanoparticles was examined by XRD analysis as shown in Fig. 2. The XRD pattern revealed sharp peaks, indicating high degree of crystallinity except for Zn₂Ni, which had comparatively broad peaks showing reduced crystallinity and smaller crystallite size [27]. The XRD pattern of all samples matched closely with their characteristic peaks according to the data base of the Joint Committee on Powder Diffraction Standards (JCPDS). Hexagonal ZnO (JCPDS # 36-1451), monoclinic CuO (JCPDS # 05-0661), cubic NiO (JCPDS # 78-0643), cubic ZrO₂ (JCPDS # 27-0997) and cubic CeO₂ (JCPDS # 81-0792) were the major phases detected in the XRD patterns. For pure ZnO, the diffraction peaks were located at $2\theta=31.84^{\circ}$, 34.52°, 36.33°, 47.63°, 56.71°, 62.96°, 68.13°, and 69.18° that are associated with (100), (002), (101), (102), (110), (103), (112) and (201) planes, respectively. The lack of peak shifts in the XRD pattern of coupled metal oxides indicates that other metal oxide is

present on the surface of ZnO and it does not get substituted in to ZnO lattice [28]. The crystallite size of ZnO and coupled metal oxides was calculated using the Debye-Scherrer formula, $d=0.89\lambda/\beta\cos\theta$ [29], where 'd' is the crystallite size, 0.89, Scherrer's constant, λ, the wavelength of X-rays, θ, the Bragg diffraction angle, and β, the full width at half-maximum (FWHM) of the diffraction peak. The crystallite size along with the calculated lattice parameters are tabulated in Table 1. Compared to individual ZnO, the coupled metal oxides showed decreased crystallite sizes. Lattice parameters of ZnO and the coupled metal oxides vary slightly, which suggests intra-granular coupling in the coupled oxides [30].

1-2. UV-vis DRS Analysis

The diffuse reflectance spectra of individual metal oxides ZnO, CuO, NiO, ZrO₂, CeO₂ and the coupled oxides Zn₂Cu, Zn₂Ni, Zn₂Zr and Zn₂Ce were examined in the range of 200-800 nm at room temperature to figure out their optical absorption properties. The reflectance spectra were interpreted using a modified Kubelka-Munk function F(R) [31], from the following equation: $F(R)=(1-R)^2/2R$ where F(R) is the Kubelka-Munk function and R is the reflectance. A graph was plotted between $(F(R)h\upsilon)^2$ and $h\upsilon$, and the intercept value obtained corresponds to the band gap energy. Fig. 3 shows the UV-Vis DRS plots for pure ZnO and the coupled oxides. The synthesized ZnO nanoparticles show band gap energy of 3.17 eV. Coupling with metal oxides like CuO, NiO, ZrO₂ and CeO₂ leads to a red shift of ZnO band gap. The band gap values are compiled in Table 1. The band gap depends on the crystalline structure and the defects in the metal oxide framework. The red shift in the optical band gap might be caused by the stoichiometry deficiency of ZnO, due to coupling with MO [20].

UV-Vis diffuse reflectance absorption spectra of pure and coupled oxides as displayed in Fig. 4 showed that the absorption edges of the coupled oxides are shifted toward the lower energy region and to longer wavelengths in comparison with pure ZnO. Zn₂Ce showed maximum absorption in the UV region, whereas Zn₂Cu and Zn₂Ni showed better absorption in the visible region. UV-Vis DRS plots for pure CuO, NiO, ZrO₂ and CeO₂ are shown as Fig. 5. The band gap values are calculated for these metal oxides to determine the conduction and valence band positions.

1-3. Photoluminescence (PL) Analysis

PL signals result from the recombination of charge carriers: The stronger the band-band PL signal, the higher will be the recombination rate of photo-induced carriers. PL spectrum can reveal important information about the surface defects, oxygen vacancies and surface states, which can strongly affect the photocatalytic reactions [32]. Fig. 6 shows the PL spectra of individual ZnO and cou-

Table 1. Crystallite size, lattice parameters, band gap, rate constant and R² values of ZnO and coupled ZnO catalysts

Photocatalyst	Crystallite size (nm)	Lattice parameter (nm)		Band gap (eV)	Rate constant (k)	Regression coefficient (R²)
		a=b	c			
ZnO	45	0.3254	0.5212	3.17	0.007	0.9924
Zn₂Cu	26-37	0.3251	0.5208	2.94	0.008	0.9971
Zn₂Ni	11-31	0.3250	0.5206	2.90	0.009	0.9953
Zn₂Zr	25-34	0.3245	0.5201	3.13	0.010	0.9977
Zn₂Ce	23-30	0.3247	0.5202	3.14	0.013	0.9971

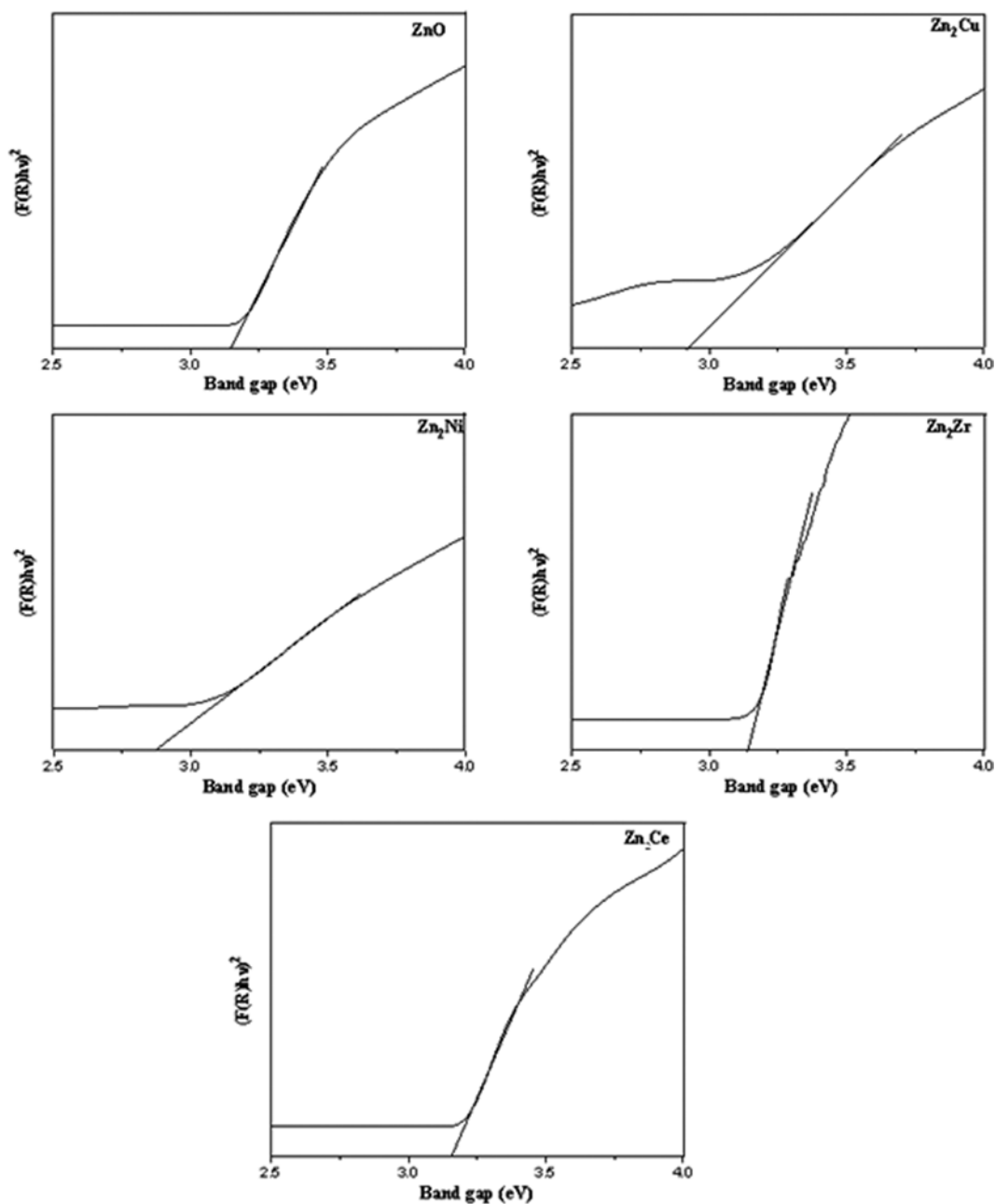**Fig. 3. UV-visible DRS plots of ZnO and the coupled oxides Zn₂Cu, Zn₂Ni, Zn₂Zr, Zn₂Ce.**

pled oxides at the excitation wave length of 320 nm. The intense emission observed around 390 nm for ZnO and the coupled metal oxides results from the radiative recombination of an excited electron in the conduction band with the hole in the valence band or the near band edge emission. The blue-green emissions at 435 and 460-580 nm are due to the excitonic PL signals where the non-radiative transitions of excited electrons from the CB bottom to different sub-bands caused by the surface oxygen vacancies and the defects in the semiconductors occur first, followed by the radiative transitions from the sub-band to VB. The oxygen vacancies can promote O_2 adsorbing and the adsorbed O_2 can capture photo-induced electrons and produce O_2 radical groups. These radical groups are active to promote the oxidation of organic substances [32]. PL emis-

sion intensity of coupled metal oxides is less compared to pure ZnO. This is attributed to the suppression of recombination of photo-generated electron-hole pairs in the coupled metal oxides as the excited electrons are involved in interparticle electron transfer process [33]. The coupled metal oxide, Zn₂Ce showed lowest PL emission intensity indicating efficient interparticle electron/hole transfer between ZnO and CeO₂.

1-4. Morphology and Size Analysis

The surface morphology of the as-prepared ZnO and coupled metal oxides, Zn₂Cu, Zn₂Ni, Zn₂Zr and Zn₂Ce was examined by FESEM analysis. Growth of the nanoparticles cannot be controlled in the combustion synthesis so that particles with varying sizes are obtained. Fig. 7(a) shows the SEM micrograph of ZnO
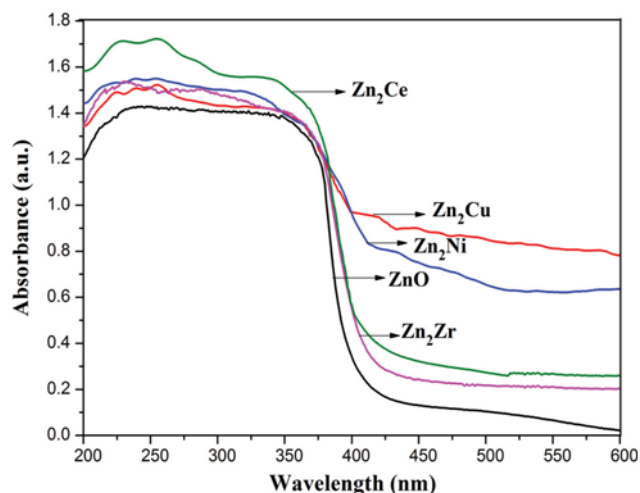
Fig. 4. UV-visible diffuse reflectance absorption spectra of ZnO and the coupled oxides Zn$_2$Cu, Zn$_2$Ni, Zn$_2$Zr, Zn$_2$Ce.

Fig. 6. Photoluminescence spectra of ZnO and the coupled oxides Zn$_2$Cu, Zn$_2$Ni, Zn$_2$Zr, Zn$_2$Ce.

nanoparticles, which are of irregular spherical shape with varying sizes between 50-150 nm. Fig. 7(b), (c), (d) and (e) shows the SEM micrographs of coupled metal oxides, Zn$_2$Cu, Zn$_2$Ni, Zn$_2$Zr and Zn$_2$Ce, respectively, with sizes ranging from 10-150 nm. In the coupled metal oxides, the respective metal oxides (CuO, NiO, ZrO$_2$ and CeO$_2$) are embedded on the matrix of ZnO nano particles. The SEM images show that the particles are aggregated, which is due

to the enormous heat generated during the combustion reaction.

Energy dispersive X-ray analysis (EDX) was carried out to determine the elemental composition of the prepared ZnO and coupled metal oxides, Zn$_2$Cu, Zn$_2$Ni, Zn$_2$Zr and Zn$_2$Ce, which are shown in Fig. 8(a)-(e). From the EDX result, only the respective elements
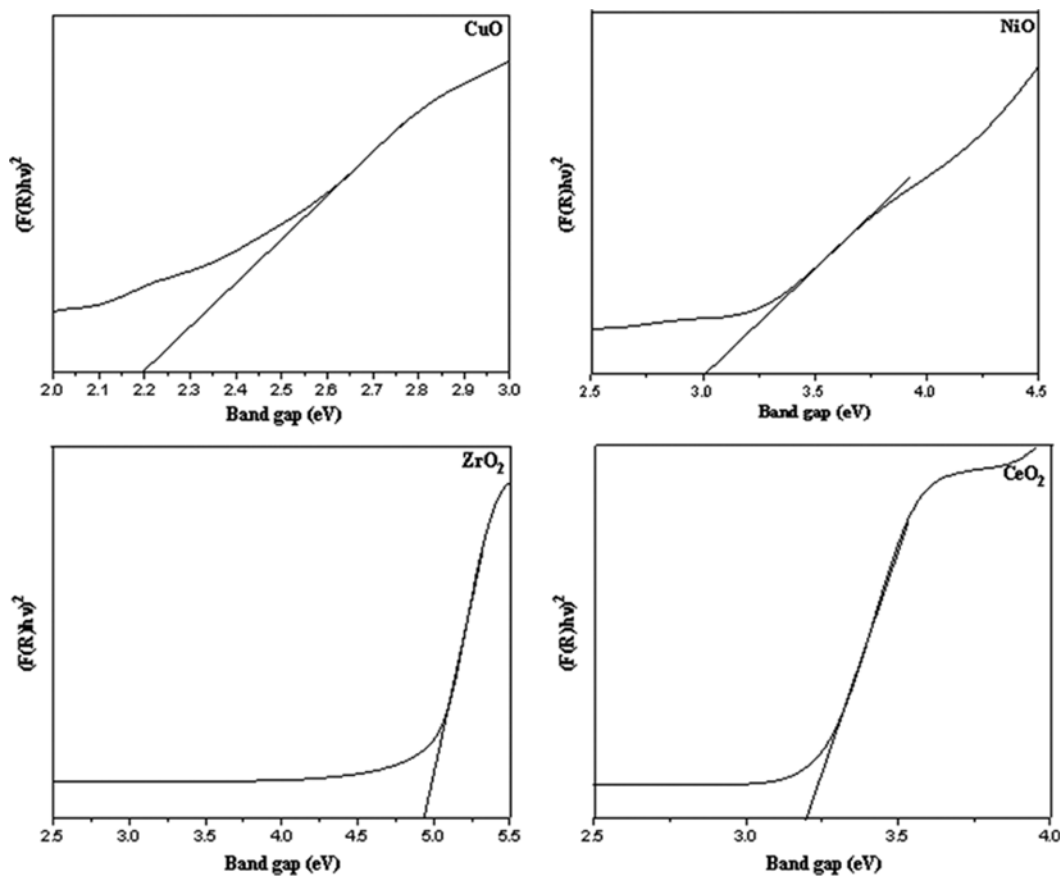

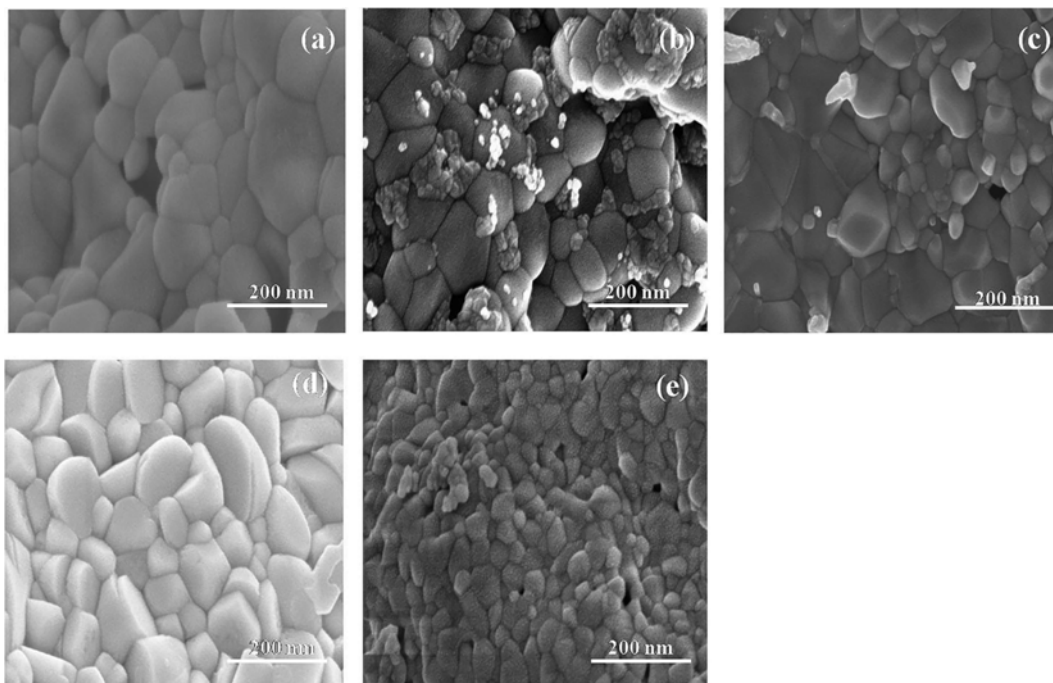Fig. 5. UV-visible DRS plots of CuO, NiO, ZrO$_2$ and CeO$_2$.

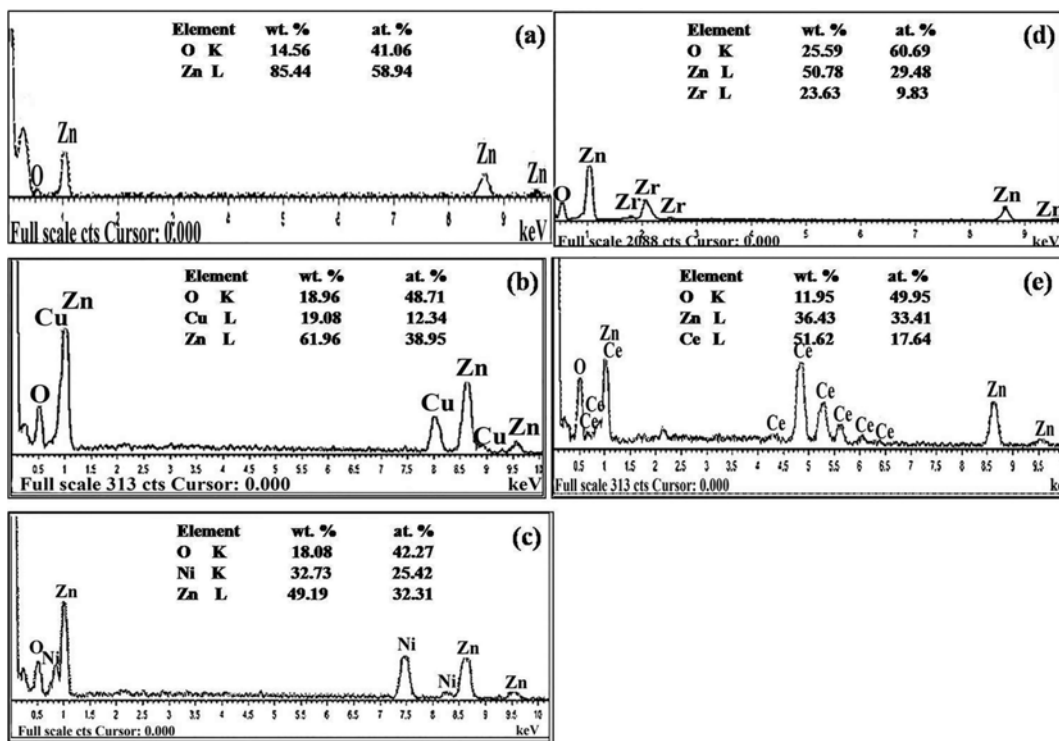Fig. 7. FESEM images of (a) ZnO, (b) Zn₂Cu, (c) Zn₂Ni, (d) Zn₂Zr, (e) Zn₂Ce.

Fig. 8. EDX spectra of (a) ZnO, (b) Zn₂Cu, (c) Zn₂Ni, (d) Zn₂Zr, (e) Zn₂Ce.

with the corresponding characteristic peaks and compositions were detected. Absence of extra peaks clearly indicates that the prepared samples are free from impurities. The compositions of pure ZnO as well as the coupled oxides revealed oxygen deficiency.

Fig. 9(a)-(e) displays the TEM images of pure ZnO and coupled oxides, Zn_2Cu, Zn_2Ni, Zn_2Zr and Zn_2Ce, respectively. Fig. 9(a) shows spherical particles of ZnO with sizes in the range of 40-50 nm. TEM images of coupled metal oxides (Fig. 9(b)-(e)) show larger irregular spherical particles of ZnO with sizes in the range of 20-40 nm interspersed with smaller particles of the other metal oxide
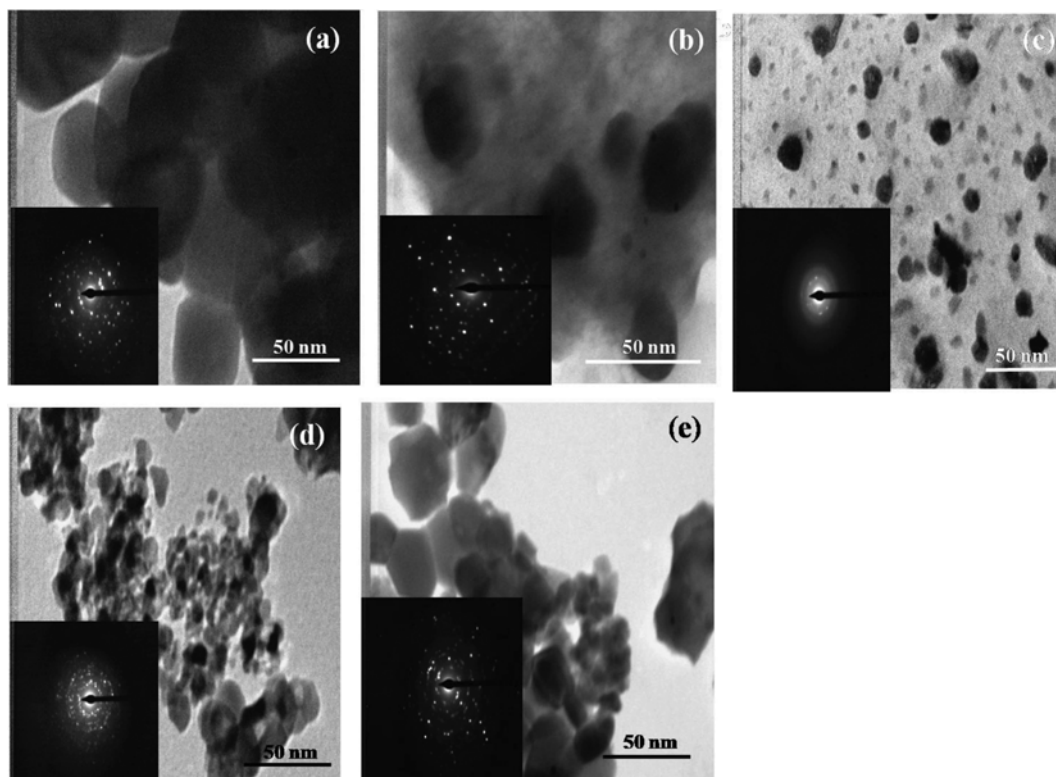
Fig. 9. TEM images of (a) ZnO, (b) Zn$_2$Cu, (c) Zn$_2$Ni, (d) Zn$_2$Zr, (e) Zn$_2$Ce (SAED pattern is shown as inset).

(CuO, NiO, ZrO$_2$ and CeO$_2$). The sizes of CuO, NiO, ZrO$_2$ and CeO$_2$ range between 5-25 nm. On coupling with other metal oxides, the growth of ZnO particle is inhibited. This causes a particle size decrease in the coupled oxides with an increase in the specific surface area [34].

1-5. Brunauer-Emmett-Teller (BET) Surface Area Analysis

The surface area (S$_{BET}$) of ZnO and the coupled oxides were determined by nitrogen physisorption technique using the BET method. Compared to pure ZnO, the coupled oxides showed higher surface area. BET surface area of pure ZnO and the coupled oxides Zn$_2$Cu, Zn$_2$Ni, Zn$_2$Zr and Zn$_2$Ce were determined to be 9.46, 10.83, 11.65, 13.37 and 14.26 m^2 g^{-1}, respectively. This contributed to the enhanced photocatalytic activity of coupled oxides over ZnO and the coupled oxide Zn$_2$Ce with the largest surface area showed the highest photocatalytic activity.

1-6. FTIR Spectra

Fig. 10 displays the FTIR spectra of pure ZnO and coupled ZnO. All the samples have a peak around 3,400 cm^{-1}, which corresponds to the stretching of surface OH$^-$ groups on the metal oxide [35]. The photocatalytic activity is closely associated with the amount of OH$^-$ groups on the catalyst, because they can capture the photogenerated hole and can get transformed to reactive ·OH radical. The peak around 1,650 cm^{-1} was assigned to the bending vibration of adsorbed H$_2$O on the surface of the catalyst [35]. Pure ZnO spectrum was dominated by the band at 430 cm^{-1}, which can be ascribed to the stretching of Zn-O bond. For the coupled metal oxides, a broad peak in the range of 440-570 cm^{-1} is due the combined absorption of Zn-O and M-O bonds [36,37]. Less intense
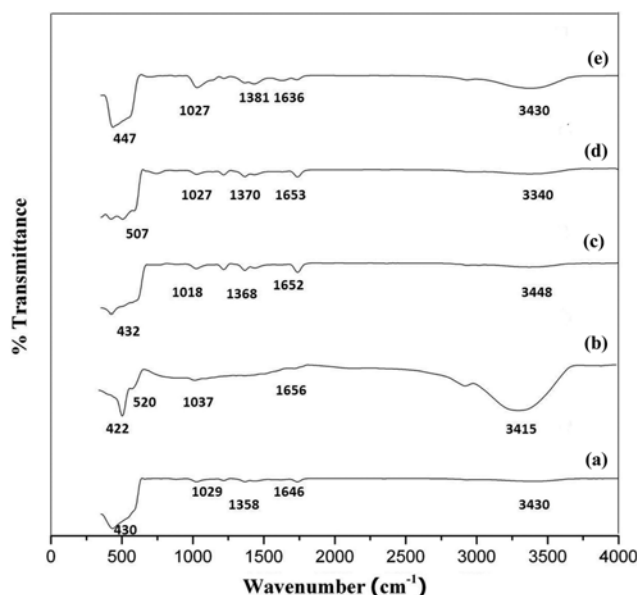

Fig. 10. FTIR spectra of (a) ZnO, (b) Zn$_2$Cu, (c) Zn$_2$Ni, (d) Zn$_2$Zr, (e) Zn$_2$Ce.

peaks observed around 1,030 cm^{-1} and 1,360 cm^{-1} are assigned to the C-O and O-C-O stretching modes respectively of the carbonate species formed on the surface of the catalysts from the adsorbed CO$_2$ [38].

2. Photocatalytic Activity

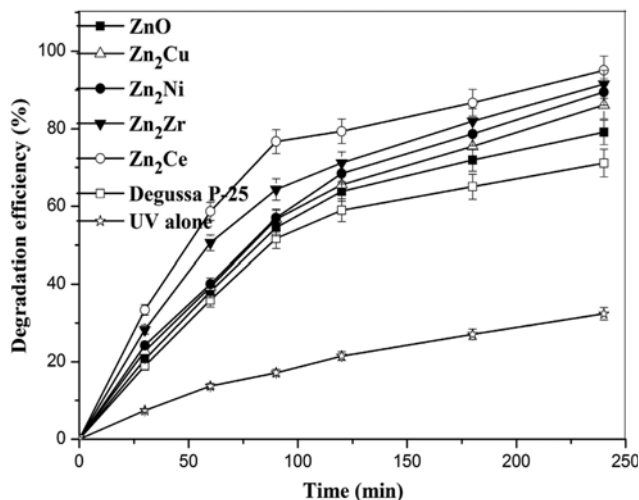The photocatalytic activity of pure ZnO and coupled oxides

Fig. 11. PCD efficiency of coupled oxides Zn₂Cu, Zn₂Ni, Zn₂Zr and Zn₂Ce in comparison with ZnO, Degussa P-25 and UV radiation alone.

Fig. 13. Kinetic curves of In(C₀/Cₜ) Vs. irradiation time for ZnO and the coupled oxides Zn₂Cu, Zn₂Ni, Zn₂Zr, Zn₂Ce.

was tested for the degradation of 2,4-dichlorophenol (2,4-DCP). Photocatalytic degradation (PCD) was carried out with an initial 2,4-DCP concentration of 50 mgL^{-1}, catalyst concentration of 50 mg/100 mL, pH around 6.5 for an irradiation time of 240 min over ZnO and the coupled oxides, Zn₂Cu, Zn₂Ni, Zn₂Zr and Zn₂Ce. On irradiation with near UV light (365 nm), the coupled oxide catalysts displayed improved photocatalytic activity when compared to pure ZnO and maximum degradation was obtained with Zn₂Ce (96%) as shown in Fig. 11. The degradation efficiency of coupled oxides was also compared with that of Degussa P-25. There was limited degradation in the absence of any catalyst with UV irradiation alone. Fig. 12 presents the UV-visible absorption spectra of 2,4-DCP after stirring in the dark for 30 minutes in the presence of ZnO and the coupled oxides. There was a small decrease in the intensity of absorption peaks of 2,4-DCP; this decrease is much pronounced with Zn₂Ce (7%) followed by Zn₂Zr (6%),
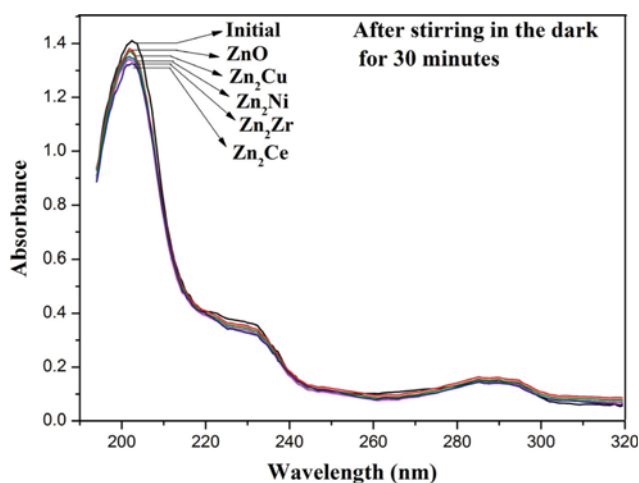
owing to their higher surface area, thus facilitating the improved adsorption of 2,4-DCP.

The better photocatalytic activity of coupled metal oxides could be due to the interparticle electron transfer between ZnO and MO and the smaller particle size, and thus the larger surface area of coupled oxides compared to pure ZnO. The photocatalytic degradation obeyed the first-order reaction kinetics as described by the equation, $\ln(C_0/C_t)=kt$, where, C_0 is the initial concentration of 2,4-DCP at t=0 min, C_t, the concentration of 2,4-DCP at irradiation time 't' and k is the rate constant [39]. The plot of ln (C_0/C_t) versus irradiation time 't' is depicted in Fig. 13 and a linear relationship is observed. First-order rate constants are evaluated from the slopes of $\ln(C_0/C_t)$ versus time plots. The rate constants with regression coefficient (R^2) are given in Table 1.

3. Proposed Mechanism for the Enhanced Photocatalytic Degradation

On coupling ZnO with another metal oxide, there arises transport of e⁻ and h⁺ between the two semiconductors, based on the relative energy band positions of the metal oxide and ZnO. The band positions of metal oxides are calculated based on the method used by Xu and Schoonen [40]. The band gap values of individual metal oxides are obtained from the DRS study as given in Fig. 3 and 5.

According to the thermodynamic requirement, the valence band (VB) and conduction band (CB) of the semiconductor photocatalyst should be positioned in such a way that the oxidation potential of the hydroxyl radicals (E⁰ (H₂O/OH•=2.8 V vs NHE) and the reduction potential of superoxide radicals (E⁰ (O₂/O₂•⁻)=−0.28 V vs NHE) lie well within the band gap. The redox potential of the VB hole must be sufficiently positive to generate hydroxyl radicals and that of the CB electron must be sufficiently negative to generate superoxide radicals [41].

ZnO and the coupled metal oxides were irradiated with UV light (365 nm). For ZnO/CuO coupled oxide, the CB and VB of the CuO are located between those of the ZnO (Fig. 14). Under near UV light irradiation, electronic excitation takes place in ZnO

Fig. 12. Change in the absorption spectrum of 2,4-DCP after stirring in the dark for 30 minutes with ZnO, Zn₂Cu, Zn₂Ni, Zn₂Zr and Zn₂Ce.
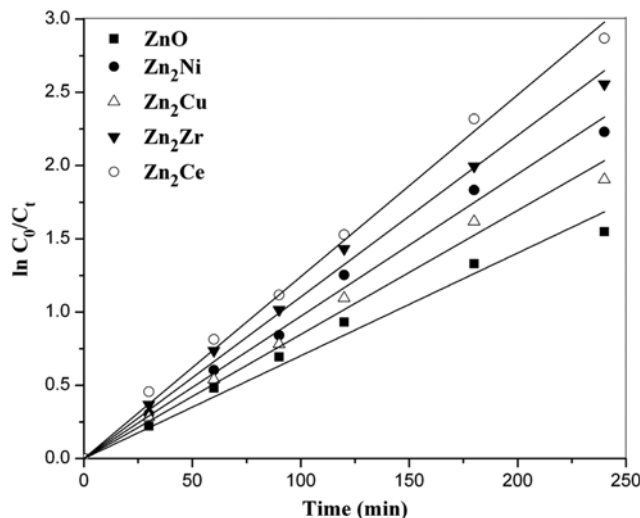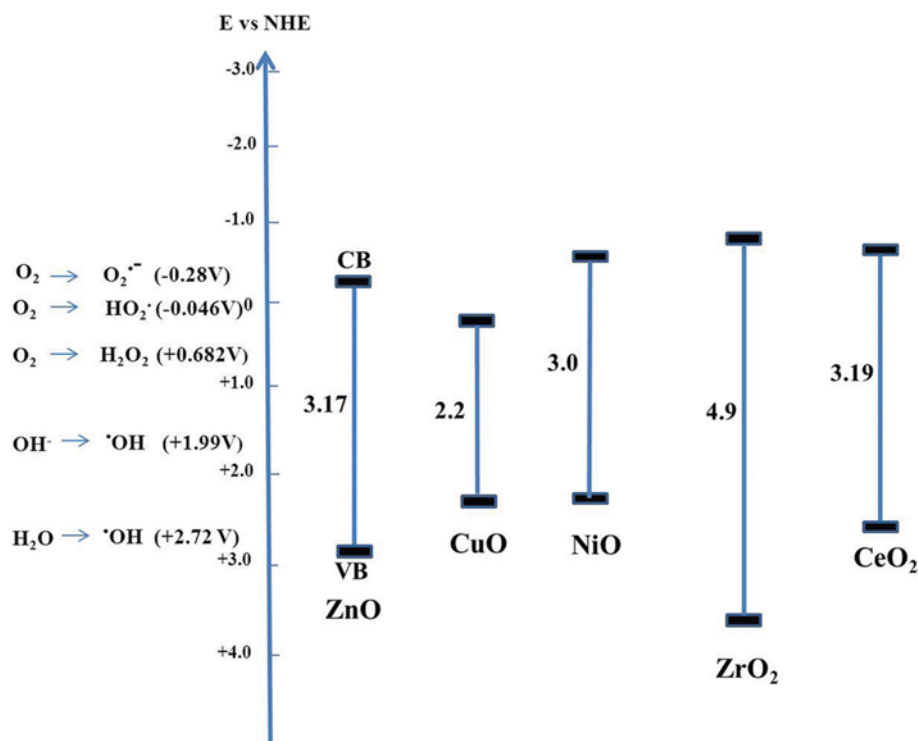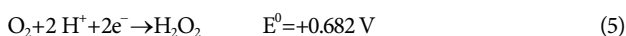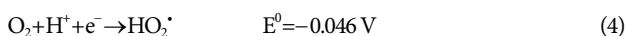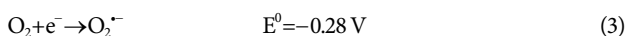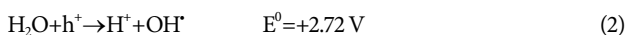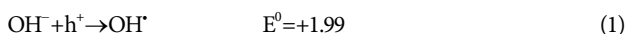
Fig. 14. Schematic of the energy band positions of ZnO, CuO, NiO, ZrO₂ and CeO₂.

and CuO and the excited e^- from the CB of ZnO is transferred to the CB of CuO as the CB position of CuO lies lower than that of ZnO. Simultaneously, the h^+ in VB of the ZnO is also transferred to the VB of CuO. The h^+ in the VB of CuO can oxidize OH^- as shown in Eq. (1). There is increased e^-/h^+ recombination on CuO because of its narrow band gap [42]. As a result, ZnO coupling with CuO did not show expected UV light photocatalytic activity.

$$OH^- + h^+ \rightarrow OH^\bullet \qquad E^0 = +1.99 \qquad (1)$$

$$H_2O + h^+ \rightarrow H^+ + OH^\bullet \qquad E^0 = +2.72\ V \qquad (2)$$

$$O_2 + e^- \rightarrow O_2^{\bullet-} \qquad E^0 = -0.28\ V \qquad (3)$$

$$O_2 + H^+ + e^- \rightarrow HO_2^\bullet \qquad E^0 = -0.046\ V \qquad (4)$$

$$O_2 + 2\ H^+ + 2e^- \rightarrow H_2O_2 \qquad E^0 = +0.682\ V \qquad (5)$$

NiO is a p-type semiconductor having a bandgap around 3 eV with CB position at -0.5 eV (Vs. NHE) and VB at $+2.5$ eV (Vs.NHE) [40]. In ZnO/NiO heterojunction (Fig. 14), the CB of NiO lies more negative than the CB of ZnO and its VB lies less positive than VB of ZnO. Thereby, e^- from CB of NiO can be transferred to CB of ZnO and h^+ from the VB of ZnO can be transferred to that of NiO. However, the h^+ in the VB of NiO cannot oxidize H_2O to $OH^\bullet$ radical as per Eq. (2) due to the VB position of NiO. Though there is interparticle e^-/h^+ transfer, photocatalytic degradation is less effective on this coupled oxide. Poor crystallinity could be another reason for the low photocatalytic degradation efficiency on Zn₂Ni [43].

Though ZrO₂ has a band gap of 4.9 eV, it showed some photocatalytic activity at 365 nm, and this must be due to electronic excitation taking place through the defect energy levels present in the

band gap or through the phenol sensitized excitation as discussed in our previous publication [44]. The coupled oxide, Zn₂Zr showed a band gap of 3.13 eV. In ZnO/ZrO₂ heterojunction, the VB of ZrO₂ is at $+3.66$ V and its CB is at -0.84 V. The VB hole is positive enough to generate hydroxyl radicals and its CB electron is negative enough to generate the superoxide radicals. Once the electron is excited to the CB of ZrO₂ it can be transferred to the CB of ZnO as it lies lower. The holes generated in the VB of ZrO₂ are also transferred to the VB of ZnO as it lies more negative than that of ZrO₂. Though there is limited electronic excitation on ZrO₂ at 365 nm irradiation, electron-hole pair recombination is slow, due to the wide band gap of ZrO₂. The transferred electrons and holes on ZnO surface can cause the oxidation of 2,4-DCP through the efficient generation of hydroxyl radicals as per Eqs. (1) to (5).

In the ZnO/CeO₂ heterojunction, the CB of CeO₂ is positioned more negative than that of ZnO (Fig. 14). On irradiation with near UV light, both ZnO and CeO₂ are excited and the photo-excited e^- from the CB of CeO₂ will be transferred to CB of ZnO as it lies lower. Meanwhile, the holes will flow from the VB of ZnO to the VB of CeO₂. The electrons in the CB of ZnO can induce various reduction reactions and generate superoxide radical ($O_2^{\bullet-}$), hydroperoxyl radical ($HO_2^\bullet$) and hydrogen peroxide (H_2O_2) as per Eqs. (3), (4) and (5) and these in turn can generate $OH^\bullet$ and degrade 2,4-DCP [45]. The h^+ in the valence band of CeO₂ can induce direct oxidation of 2,4-DCP or degrade it through $OH^\bullet$ generated as per Eqs. (1) and (2). The order of photocatalytic activity of the as-synthesized samples was ZnO/CeO₂>ZnO/ZrO₂>ZnO/NiO> ZnO/CuO>pure ZnO. Electron-hole pair recombination was minimum on ZnO/CeO₂, followed by ZnO/ZrO₂, ZnO/NiO, ZnO/CuO as indicated by the PL studies. Recombination of e^-/h^+ pairs was

maximum on ZnO as indicated by the intense PL signals.

CONCLUSIONS

ZnO and its coupled oxides with CuO, NiO, ZrO$_2$ and CeO$_2$ has were synthesized by the microwave-assisted combustion method and successfully characterized by XRD, FT-IR, SEM, TEM, EDX, BET, UV-Vis DRS and PL analysis. Coupling with these metal oxides has decreased the crystallite size of ZnO. XRD, SEM, TEM and EDX measurements confirmed coupling of ZnO with the respective metal oxide. Coupled ZnO displayed improved photocatalytic activity towards the degradation of 2,4-dichloro phenol under irradiation with near UV light, and maximum degradation was obtained with Zn$_2$Ce. The enhancement of the photocatalytic activity was mainly attributed to the inter-semiconductor e$^-$ and h$^+$ transfer as shown by the PL measurements and due to the reduced particle size in the coupled oxides.

REFERENCES

1. E. Evgenidou, K. Fytianos and I. Poulios, *Appl. Catal., B*, **59**, 81 (2005).
2. J. R. T. Hernandez, E. R. Morales, L. R. Blanco, J. P. Enriquez, G. Oskam, F. P. Delgado, B. E. Morales, M. A. Alejandro, L. L. D. Flores and G. P. Hernandez, *Mater. Sci. Semicond. Process*, **37**, 87 (2015).
3. S. Sakthivel, B. Neppolian, M. V. Shankar, B. Arabindoo, M. Palanichamy and V. Murugesan, *Sol. Energy Mater. Sol. Cells*, **77**, 65 (2003).
4. J. C. Sin, S. M. Lam, K. T. Lee and A. R. Mohamed, *J. Colloid Interface Sci.*, **401**, 40 (2013).
5. Y. Ao, J. Xu, D. Fu and C. Yuan, *Micropor. Mesopor. Mater.*, **122**, 1 (2009).
6. H. Zhang, R. Zong, J. Zhao and Y. Zhu, *Environ. Sci. Technol.*, **42**, 3803 (2008).
7. Q. Wang, C. Chen, D. Zhao, W. Ma and J. Zhao, *Langmuir*, **24**, 7338 (2008).
8. K. Tennakone and J. Bandara, *Appl. Catal. A: Gen.*, **208**, 335 (2001).
9. W. Cun, Z. Jincai, W. Xinming, M. Bixian, S. Guoying, P. Ping'an and F. Jiamo, *Appl. Catal. B: Environ.*, **39**, 269 (2002).
10. Y. U. Changlin, Y. Kai, S. Qing, Y. U. Jimmy, C. A. O. Fangfang and L. Xin, *Chin. J. Catal.*, **32**, 555 (2011).
11. J. Wang, P. Liu, X. Fu, Z. Li, W. Han and X. Wang, *Langmuir*, **25**, 1218 (2008).
12. X. Zhang, J. Qin, Y. Xue, P. Yu, B. Zhang, L. Wang and R. Liu, *Sci. Rep.*, **4**, 4596 (2014).
13. P. Chen, T. Y. Xiao, H. H. Li, J. J. Yang, Z. Wang, H. B. Yao, and S. H. Yu, *ACS Nano*, **6**, 712 (2011).
14. N. Zhang, Y. Zhang, M. Q. Yang, Z. R. Tang and Y. J. Xu, *J. Catal.*, **299**, 210 (2013).
15. J. X. Sun, Y. P. Yuan, L. G. Qiu, X. Jiang, A. J. Xie, Y. H. Shen and J. F. Zhu, *Dalton Trans.*, **41**, 6756 (2012).
16. X. Bai, L. Wang, R. Zong, Y. Lv, Y. Sun and Y. Zhu, *Langmuir*, **29**, 3097 (2013).
17. M. M. Hossain, B. C. Ku and J. R. Hahn, *Appl. Surf. Sci.* (2015), DOI:10.1016/j.apsusc.2015.01.191.
18. R. Saravanan, S. Karthikeyan, V. K. Gupta, G. Sekaran, V. Narayanan and A. Stephen, *Mater. Sci. Eng. C*, **33**, 91 (2013).
19. J. Gajendiran and V. Rajendran, *Mater. Lett.*, **116**, 311 (2014).
20. P. Sathishkumar, R. Sweena, J. J. Wu and S. Anandan, *Chem. Eng. J.*, **171**, 136 (2011).
21. K. A. Singh, L. C. Pathak and S. K. Roy, *Ceram. Int.*, **33**, 1463 (2007).
22. J. Li, Y. B. Pan, F. G. Qiu, Y. S. Wu and J. K. Guo, *Ceram. Int.*, **34**, 141 (2008).
23. R. D. Purohit, B. P. Sharma, K. T. Pillai and A. K. Tyagi, *Mater. Res. Bull.*, **36**, 2711 (2001).
24. J. Jia, S. Zhang, P. Wang and H. Wang, *J. Hazard. Mater.*, **205-206**, 150 (2012).
25. M. P. Titus, V. G. Molina, M. A. Banos, J. Gimenez and S. Esplugas, *Appl. Catal. B: Environ.*, **47**, 219 (2004).
26. S. Chaliha and K. G. Bhattacharyya, *J. Chem. Eng.*, **139**, 575 (2008).
27. B. Ohtani, *J. Photochem. Photobiol. C*, **11**, 157 (2010).
28. B. Krishnakumar, T. Imae, J. Miras and J. Esquena, *Sep. Purif. Technol.*, **132**, 281 (2014).
29. B. D. Cullity, *Elements of X-ray diffraction*, Addison-Wesley, Reading, Mass, USA, 3rd Ed. (1967).
30. R. Saravanan, N. Karthikeyan, V. K. Gupta, E. Thirumal, P. Thangadurai, V. Narayanan and A. Stephen, *Mater. Sci. Eng. C*, **33**, 2235 (2013).
31. P. Ji, J. Zhang, F. Chen and M. Anpo, *J. Phys. Chem. C*, **112**, 17809 (2008).
32. J. Liqiang, Q. Yichun, W. Baiqi, L. Shudan, J. Baojiang, Y. Libin, F. Wei, F. Honggang and S. Jiazhong, *Mater. Sol. Cells*, **90**, 1773 (2006).
33. S. Sakthivel, S. U. Geissen, D. W. Bahnemanna, V. Murugesan and A. Vogelpohl, *J. Photochem. Photobiol. A: Chem.*, **148**, 283 (2002).
34. C. Shifu, Z. Sujuan, L. Wei and Z. Wei, *J. Hazard. Mater.*, **155**, 320 (2008).
35. G. S. Pozan, M. Isleyen and S. Gokcen, *Appl. Catal. B Environ.*, **140-141**, 537 (2013).
36. C. Li, R. Chen, X. Zhang, S. Shu, J. Xiong, Y. Zheng and W. Dong, *Mater. Lett.*, **65**, 1327 (2011).
37. M. Faisal, S. B. Khan, M. M. Rahman, A. Jamal, K. Akhtar and M. M. Abdullah, *J. Mater. Sci. Technol.*, **27**, 594 (2011).
38. J. H. Taylor and C. H. Amberg, *Can. J. Chem.*, **39**, 535 (1961).
39. M. Fu, Y. Li, S. wu, P. Lu, J. Liu and F. Dong, *Appl. Surf. Sci.*, **258**, 1587 (2011).
40. Y. Xu and M. A. A. Schoonen, *Am. Mineral.*, **85**, 543 (2000).
41. R. Vinu and G. Madras, *J. Indian Inst. Sci.*, **90**, 189 (2010).
42. Y. Bessekhouad, D. Robert and J. V. Weber, *Catal. Today*, **101**, 315 (2005).
43. S. T. Nishanthi, S. Iyyapushpam, B. Sundarakannan, E. Subramanian and D. P. Padiyan, *Appl. Surf. Sci.*, **313**, 449 (2014).
44. E. D. Sherly, J. J. Vijaya, N. C. S. Selvam and L. J. Kennedy, *Ceram. Int.*, **40**, 5681 (2014).
45. S. M. Lam, J. C. Sin, A. Z. Abdullah and A. R. Mohamed, *Sep. Purif. Technol.*, **132**, 378 (2014).